Check for updates

Polyaniline-modified cobalt oxide nano-flowers for efficient electrochemical detection of nitrite

Nora Ibrahim,[a] Shymaa S. Medany, [ID] *[b] Sahar A. Fadlallah [ID] *[ab] and Mahmoud A. Hefnawy [ID] *[b]

In this work, a modified electrode containing a conducting polymer (polyaniline) with Co_2O_3 nanoflowers (NF) was constructed for efficient nitrite detection. The as-prepared $GC/Pani/Co_2O_3$-NF was characterized using various analytical techniques, including Infrared spectroscopy (IR), ultraviolet-visible spectroscopy (UV-vis), scanning electron microscopy (SEM), X-ray diffraction (XRD), atomic force microscopy (AFM), and thermal analysis (TGA/DTA) to ascertain the Co_2O_3's chemical composition and surface morphology. Furthermore, the electrode's activity toward nitrite detection was studied in a broad pH range, from 2 to 10. The linear detection range and limit were found using the amperometry approach. The $GC/Pani/Co_2O_3$-NF modified electrode displayed a linear detection range at (10–150) μM and (200–750) μM. In addition, the limits of detection, LOD, for low and high concentrations were 5.565 and 44.98 μM, respectively. While the limits of quantitation (LOQ) were 18.55, and 149.9 μM for low and high concentrations, respectively. Additionally, the kinetic properties of nitrite in different mediums were studied, including diffusion and transport coefficients. Moreover, the electrochemical impedance technique (EIS) measures the charge transfer resistance in nitrite detection upon a modified surface at various pH levels. Also, the electrode's anti-interfering properties were evaluated on a range of compounds such as (L-aspartic acid, L-methionine, L-asparagine, L-lysine, L-glutamic acid, sodium chloride, potassium chloride, glucose, and vitamin C). Antibacterial activity of polyaniline and cobalt oxide was examined to determine the biological activity. Finally, a real sample was used to test the electrode's activity (response time 4 s).

1. Introduction

Nitrite is widely used in a variety of sectors, such as fabric dyeing, meat coloring, industrial production, chemical synthesis, food preservation, and environmental preservation.[1–4] Additionally, NO_2^- is an antibacterial agent that prolongs the shelf life of perishable foods like salami, beef, and other processed meat products.[5,6] Despite these advantages, the human body may suffer from NO_2^- if too much is consumed or accumulated within the body.[7] Nitrite (NO_2^-) has become a prevalent contaminant in the environment and everyday human life. It is frequently present in artificial fertilizers, food additives, and preservatives.[8] Elevations of NO_2^- in human bodies may be highly harmful to health since they can cause methemoglobinemia and nitrosamines that can cause cancer.[9] Therefore, there's a need for effective and ongoing surveillance of the whole food supply chain due to the growing worldwide concern about food safety.

The conventional methods for identifying nitrite included colorimetric, electrochemistry, fluorescence spectroscopy, and chromatography.[10,11] Nevertheless, these methods require skilled operators and are expensive and time-consuming. The electrochemical methods are characterized by high sensitivity, ease of use, portability, and lack of production of other pollutants.[12–16] The electrochemical monitoring method has garnered more attention in identifying levels of nitrite than other methods and is thought to be more environmentally friendly.[17–19] Recent electroanalytical formats balance sensitivity and simple handling in food matrices.[20] Traditional conductive substrates exhibit poor mechanical stability and are vulnerable to the effects of electrode scale and polymer binders, which lower the rates of redox reactions on the electrode surface, despite the fact that electrochemical sensing techniques have some benefits.[21–24] Therefore, finding the right conductive substrates to facilitate electro catalysis and electro analysis is crucial. Where, signal transformation and detection are the two main phases of an electrochemical sensor's sample assessment procedure. Redox, an electrochemical reaction, is the basis of the detection method and is used to identify the substance under analysis. The molecular detection material detects the target molecule.[25]

[a]*Biotechnology Department, Faculty of Science, Cairo University, Giza, Egypt. E-mail: sahar.fadlallah@yahoo.com*

[b]*Chemistry Department, Faculty of Science, Cairo University, Giza, Egypt. E-mail: shymaasamir80@cu.edu.eg; maahefnawy@gmail.com; maadel@cu.edu.eg*

Transition metals, in the design of electrocatalysts, elements such as oxides, phosphides, nitrides, sulfides, borides, carbides, and alloys have attracted a great deal of attention.[26,27] Because of their exceptional electrocatalytic qualities, low cost, simple synthesis, and distinctive electronic configuration, transition metal oxides (TMOs), such as Co_xO_y, Ni_xO_y, Fe_xO_y, and Mo_xO_y, are showing great promise as catalysts to the oxidation of nitrite.

Because of its excellent electron transfer rate, cheap price, and environmentally friendly nature, cobalt oxide is a desirable material among transition metals. It has been used extensively in chemical modifications of the surface of electrodes in recent years.[28–30] Conducting polymers have been extensively studied due to their high sensitivity, exceptional flexibility, and controlled conductivity. These characteristics of composite materials are useful in practical applications because they might combine the superior electrochemical powers of conducting polymers with the exceptional catalytic ability of metal nanoparticles.[31,32]

The development of electrochemical detectors for nitrite detection is the main focus of this work. With a particular focus on applying polyaniline and cobalt oxide sensors in nitrite detection in food analysis. The performance of the modified electrode was investigated using different electrochemical techniques. The electrochemical method was compared with another analytical technique, such as HPLC, for the detection of nitrite in the real sample.

2. Experimental

2.1. Reagents and chemicals

Aniline, ethanol, cobalt acetate, NaCl 0.1 M, sodium nitrite, methanol, deionized water, PBS (pH 7), NaH_2PO_4, Na_2HPO_4, 1.0 N HCl, sodium per sulfate (0.1 M), and KCl. A double distillation of water was used to make each solution. All these chemicals are used as received without further purification.

2.2. Preparation of polyaniline

Double-distilled aniline was polymerized oxidatively through a standard chemical procedure to produce PANI. First, 100 mL of 1.0 N HCl was placed in an ice bath, and 5 mL of aniline was slowly added under vigorous stirring to form aniline hydrochloride. Then, 20 mL of 0.1 M sodium persulfate was gradually introduced to initiate the redox polymerization. During the reaction, a gradual color change of the solution was observed, indicating the progress of polymerization. Proper temperature control was maintained to prevent excessive heat generation from the exothermic process. After continuous stirring for four hours, the polymerization was completed. The resulting violet precipitate, identified as pernigraniline, was filtered, thoroughly washed with deionized water, and dried overnight.[33,34]

2.3. Preparation of Co_2O_3-NF

Electrochemical deposition was utilized to prepare cobalt oxide. Therefore, 50 mM cobalt acetate and 0.1 M sodium chloride were added to a glassy carbon electrode that had been modified with polyaniline. The cobalt was deposited in the potential range from -0.6 to -1.2 V (vs. Ag/AgCl) using cyclic voltammetry technique for different number of cycles (i.e., 5, 10, 15, 20 and 25) after that, the electrode was cleaned with purified water and allowed to dry overnight.

2.4. The antimicrobial and antifungal effect for cobalt oxide NFs and poly aniline materials

2.4.1. Characterization of cobalt oxide NFs and poly aniline's antimicrobial activity. The antibacterial and antifungal properties of cobalt oxide NFs and polyaniline were evaluated using an agar well diffusion technique against isolates of *Staphylococcus aureus*, *Bacillus subtilis*, (Gram positive bacteria) and *Escherichia coli* (Gram negative bacteria) by nutrient agar medium. The antifungal activity of the tested compounds was tested against *Candida albicans* using Sabouraud dextrose agar medium.[35–37] Using a sterile cotton swab, the suspension was applied to Mueller Hinton's agar. After 15 minutes, wells (6 mm) were created in the agar utilizing a sterile cork borer. Molten agar was used to seal the wells' lower ends to stop the tested nanomaterial from leaking. Add 100 μL of cobalt oxide NPs and polyaniline into each well in an equal amount using a micropipette. The inhibition zones for each fungus and microbe were measured after the Petri plates had been incubated for 24 hours at 37 °C for bacteria and 48 hours for fungi. The clean area surrounding the wells produced by the antibacterial activity of both cobalt oxide NPs and polyaniline is known as the inhibition zone. The sizes of the tested bacteria's inhibition zones were measured by the National Committee for Clinical Laboratories Standards guidelines to evaluate the antibacterial activity[38] The antibacterial activity increases with the size of the inhibition zone. Each measurement was performed three times to get an average.

2.4.2. Testing for antibiotic sensitivity. The susceptibility of *Escherichia coli*, *Staphylococcus aureus*, *Bacillus subtilis*, as well as using the disk diffusion technique on agar media, the *Candida albicans* isolates were subjected to standard antibiotics disks measuring 6 mm. Standard medications for Gram-positive and Gram-negative bacteria were ampicillin and gentamicin, respectively. Nystatin was a common medication used to treat fungal strains. DMSO was employed as a solvent (negative) control. At a dosage of 15 mg mL^{-1}, compounds were tested against strains of bacteria and fungi. A spectrophotometer set to 625 nm was used to adjust the turbidity of the microbial suspension to OD = 0.13. The suspension was made in sterile saline equal to the McFarland 0.5 standard solution (1.5×10^5 CFU mL^{-1}). A sterilized cotton swab was immersed into the modified solution and placed on the dry agar surface, ideally within 15 minutes of altering the turbidity of the inoculum suspension. The swab was left to dry for another 15 minutes with the lid in place. A sterile cork borer created wells of 6 mm in diameter in the solidified material. 100 μL of the tested compound's solution was applied to each well using a micropipette. The National Committee for Clinical Laboratories Standards guidelines were used to establish inhibition zones.[38] To get an average, each measurement was performed

three times. To evaluate the effectiveness of cobalt oxide nanoparticles and polyaniline against conventional antibiotics, the Activity Index (AI) and Fold Elevate were computed using eqn (1) and (2) based on the inhibitory diameters.[35,37] Where I_a is the antibiotic's inhibition zone diameter and I_c is the poly aniline & cobalt oxide NFs' inhibition zone diameter.

$$\text{Activity index} = \frac{I_c}{I_a} \qquad (1)$$

$$\text{Fold increase } \% = \frac{I_c - I_a}{I_a} \times 100 \qquad (2)$$

2.4.3. Analysis of statistics. The SPSS program version "22" for Windows was used to assess differences between samples of the same species of (bacteria and fungus) using one-way analysis of variance (ANOVA) and the Duncan multiple comparisons test. The values are shown as mean ± S.E., and a p-value of less than 0.05 was regarded as statistically significant, a p-value of less than 0.01 as highly significant, and a p-value of less than 0.001 as very highly significant.

2.5. Electrode fabrication and electrochemical measurements

2.5.1. Manufacturing the modified electrodes for GC/Pani/Co$_2$O$_3$-NFs. As a working electrode, an electrode made of glassy carbon (GC) with a diameter of 3 mm and a surface area of 0.0707 cm^2 was employed. It was polished with soft emery paper and then cleaned using ethanol and double-distilled water. After that, 10 milligrams of the catalyst powder (polyaniline) was dissolved in 1 mL of ethanol utilizing an ultrasonic device for one hour in order to create the cast solution for the electrocatalysts. Consequently, an altered electrode was made in the manner described below: 5 μL of Pani solution was casted onto GC elecrode's surface and allowed to dry for GC/Pani. Casting cobalt acetate (0.05 M) in a supporting (0.1 M) NaCl solution and PBS solution of (pH 7) on the modified glassy

carbon electrode's surface and letting it dry produced the GC/Pani/Co$_2$O$_3$-NF electrode. Every electrochemical measurement was performed using the Auto Lab PGSTAT128N. The impedance spectrum was matched using Metrohm Autolab's electrochemistry tool, NOVA (Version 2.1, Utrecht, Netherlands). The three-electrode system's working electrodes were GC/Pani, GC/Co$_2$O$_3$-NF, & GC/Pani/Co$_2$O$_3$-NF; Pt wire served as the reference electrode, and Ag/AgCl/KCl (sat.) served as the auxiliary electrode. Ag/AgCl/sat KCl was utilized in this study to represent all conceivable values. The Ag/AgCl/sat KCl reference electrode, which had a constant AC voltage value, was altered in the electrochemical impedance spectrum studies by applying AC voltage amplitude of 10 mV with a frequency range of 1×10^4 Hz to 0.1 Hz.

3. Results and discussion

3.1. Materials characterization and analysis

The chemical structure of prepared cobalt oxide NF was characterized by powder X-ray diffraction. The X-ray method was used to confirm the chemical structure of the produced cobalt oxide. Fig. 1 shows the XRD chart of the cobalt oxide, which shows that the cobalt sample contains Co$_2$O$_3$ with a cubic phase and a space group of ($Fd\bar{3}m$), as demonstrated by the diffraction (h, k, l) planes of (111), (220), (311), (400), (511), and (440). Coordinated with the distinctive peaks of Co$_2$O$_3$, the obtained XRD peaks match the characteristic peak design on JCPDS card number 76-1802.

The surface's morphological analysis is essential for evaluating the electrode's performance. In order to characterize the surface, scanning electron microscopy (SEM) was used. Fig. 2a–c presents the SEM of the polyaniline/cobalt oxide thin-layer composite. Fig. 2a provides a wider view of the sample's surface at 3000× magnification. It shows a surface view, different textures, and the overall morphology suggests a composite material where polyaniline and cobalt oxide are combined. In conclusion, the lower magnifications view of the
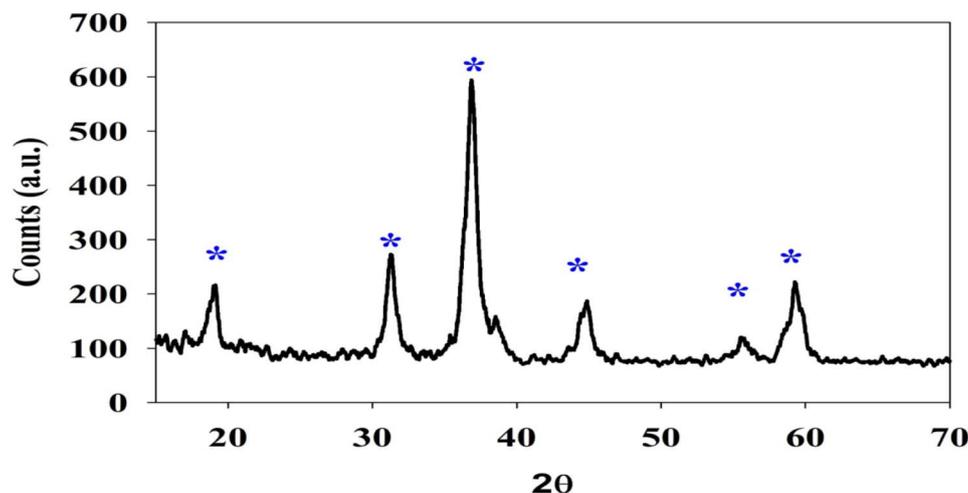

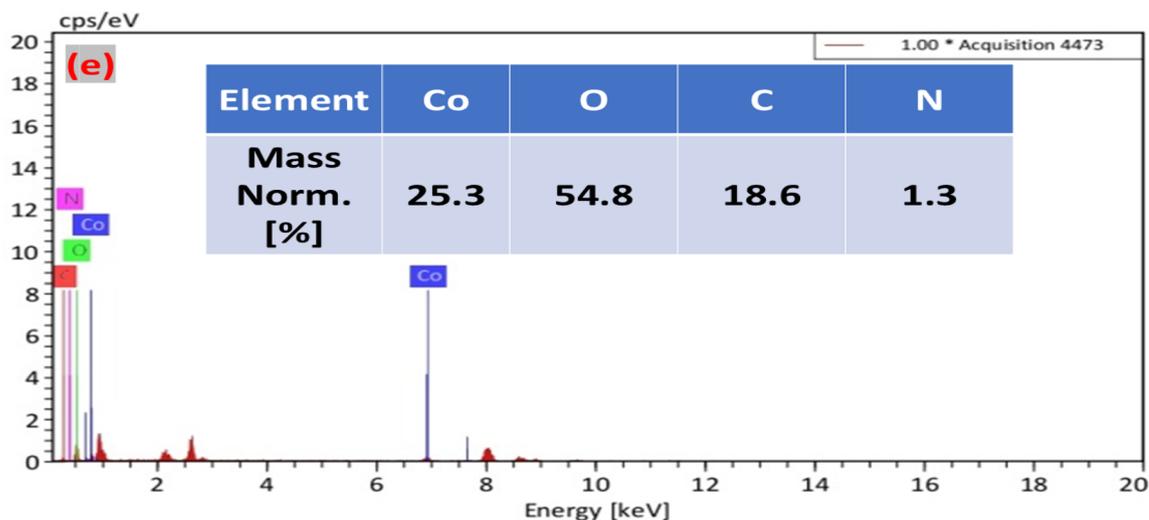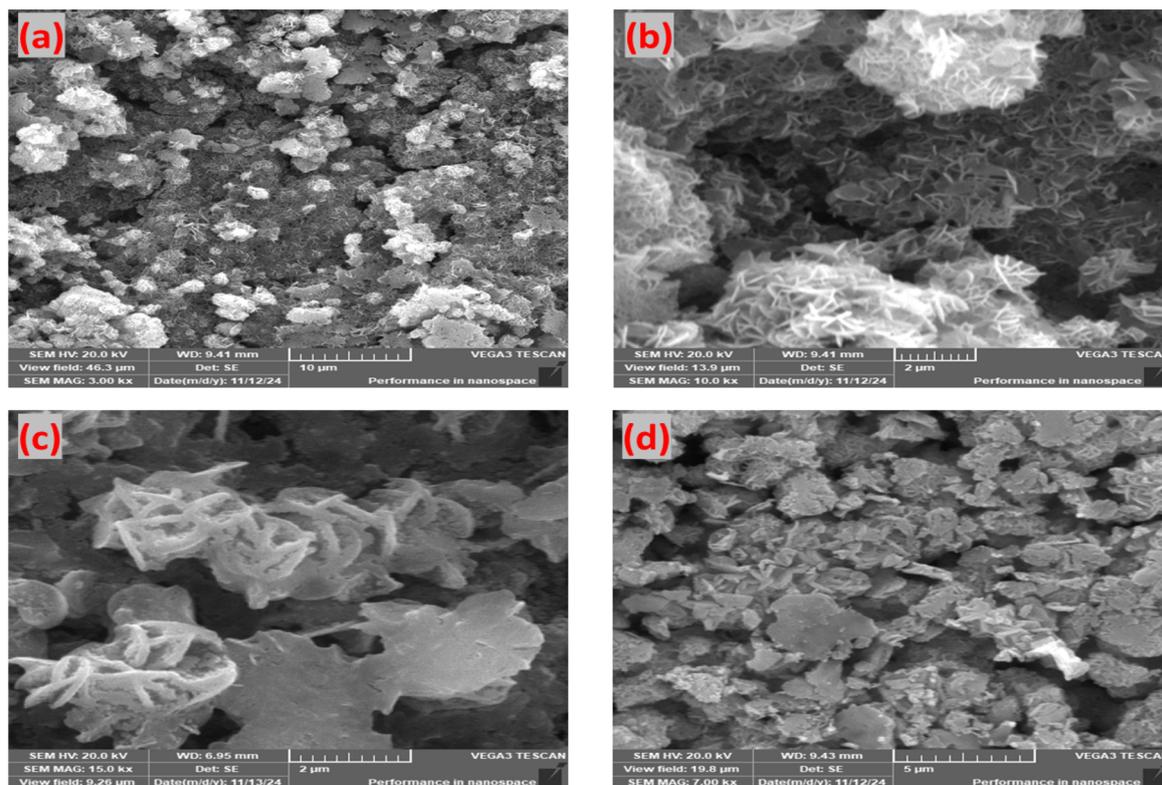Fig. 1 XRD spectrum of cobalt-oxide nanoparticles.

Fig. 2 (a–c) SEM images of polyaniline/cobalt oxide thin layer composite using different magnifications, (d) SEM OF polyaniline/cobalt oxide after detecting of nitrite (e) EDX pattern of Pani/cobalt oxide composite.

polyaniline/cobalt oxide composite, revealing its agglomerated structure and porous texture. It highlights the distribution of the material over a larger area and complements the higher magnification figure by showing the overall morphology of the composite. Fig. 2b with 10 000× magnification: this magnification provides a good balance between detail and overview, a detailed view of the surface, revealing a mix of features. The

figure shows distinct nanoscale features, including plate-like or flake-like structures and more granular or aggregated forms. The figure suggests a degree of porosity, with voids or spaces between the agglomerates. The variety of features and textures suggests a composite material combining polyaniline and cobalt oxide. This helps understand the material's structure, which is crucial for determining its properties and potential

applications. Fig. 2c, with the 15 000× magnification, reveals fine details of the composite's morphology. The figure shows distinct flower-like structures. These could be indicative of the cobalt oxide component, which often forms such structures at the nanoscale. The flower-like structures appear to be composed of nanosheets or nanoflakes. There are also more rounded or irregular particles present, which could be related to the polyaniline matrix or the interaction between the two materials. Fig. 2d shows the SEM image of Pani/cobalt oxide after detection of nitrite. Whereas, the structure of the cobalt nanoflower found to be deteriorated after contentious oxidation of the nitrite. Energy-Dispersive X-ray Spectroscopy (EDX) pattern is depicted in Fig. 2e, which is used to determine the elemental composition of a sample. The pattern exhibits several distinct peaks, corresponding to the characteristic X-ray energies of different elements in the sample. The most prominent peaks are labeled "Co", indicating presence of cobalt into the sample. Presence of these peaks confirms the presence of cobalt oxide. Other peaks were observed in the low-energy region. These peaks are likely related to elements such as nitrogen (N), oxygen (O), and potentially carbon (C), which are expected from polyaniline. The height or area under each peak is proportional to the concentration of the corresponding element. The relative peak heights can give a quantitative indication of the elemental composition. The presence of both cobalt and elements associated with polyaniline (like nitrogen) suggests the formation of composite material. The prominent cobalt peaks confirm the successful incorporation of cobalt oxide in the composite material. The presence of peaks related to nitrogen and other elements associated with polyaniline suggests that the polymer is also present in the composite. Finally, this EDX pattern confirms the presence of cobalt oxide and polyaniline in the composite material. The peaks corresponding to cobalt and other relevant elements provide evidence for the successful formation of the composite.[39]

An Atomic Force Microscopy (AFM) topographic represent of the polyaniline/cobalt oxide with thin layer composite is shown in Fig. 3. AFM provides information about the surface morphology and roughness at the nanoscale. The observed roughness suggests that the composite has a significant surface area, which can be beneficial for applications where surface interactions are important (*e.g.*, catalysis, sensing). The granular or irregular texture reflects the combined morphology of polyaniline and cobalt oxide. The agglomerates or clusters could be related to the formation of the composite material (cobalt oxide). The figure reveals a rough and textured surface, which is important for understanding the material's properties and potential applications. Furthermore, AFM study findings was found that the surface area was 0.015619 μm^2, roughness 1.310395, and Mean Radius 0.053602 μm. In line with the SEM data, these figures show that the roughness of the deposited film cycles increased as the density of cobalt oxide nanoparticles rose. Which confirms that the higher the surface roughness, the higher the electrode efficiency.

The TGA curve shows the percentage of weight remaining in a polyaniline sample as a function of temperature, providing information about its thermal stability and decomposition behavior. Initial weight loss occurs at lower temperatures, likely
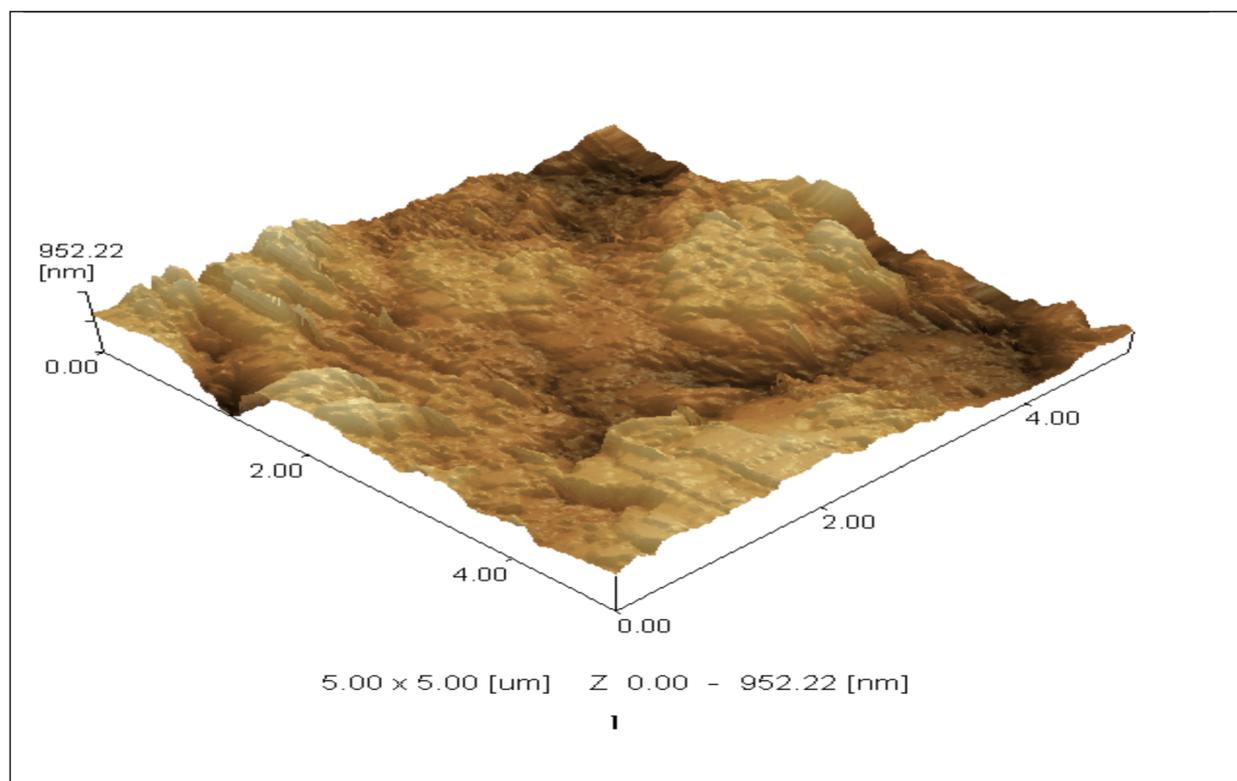

Fig. 3 AFM image of polyaniline/cobalt oxide thin layer composite.

due to moisture evaporation or residual solvents. Major decomposition occurs around 200–600 °C, indicating thermal decomposition of the polymer. Residual weight remains at higher temperatures, possibly due to the formation of carbonaceous char or inorganic residues. The derivative TGA curve

shows the rate of weight loss as a function of temperature, identifying the maximum rate of decomposition. The DTA curve shows the difference in temperature between the sample and a reference material, providing information about thermal transitions (endothermic or exothermic) occurring in the
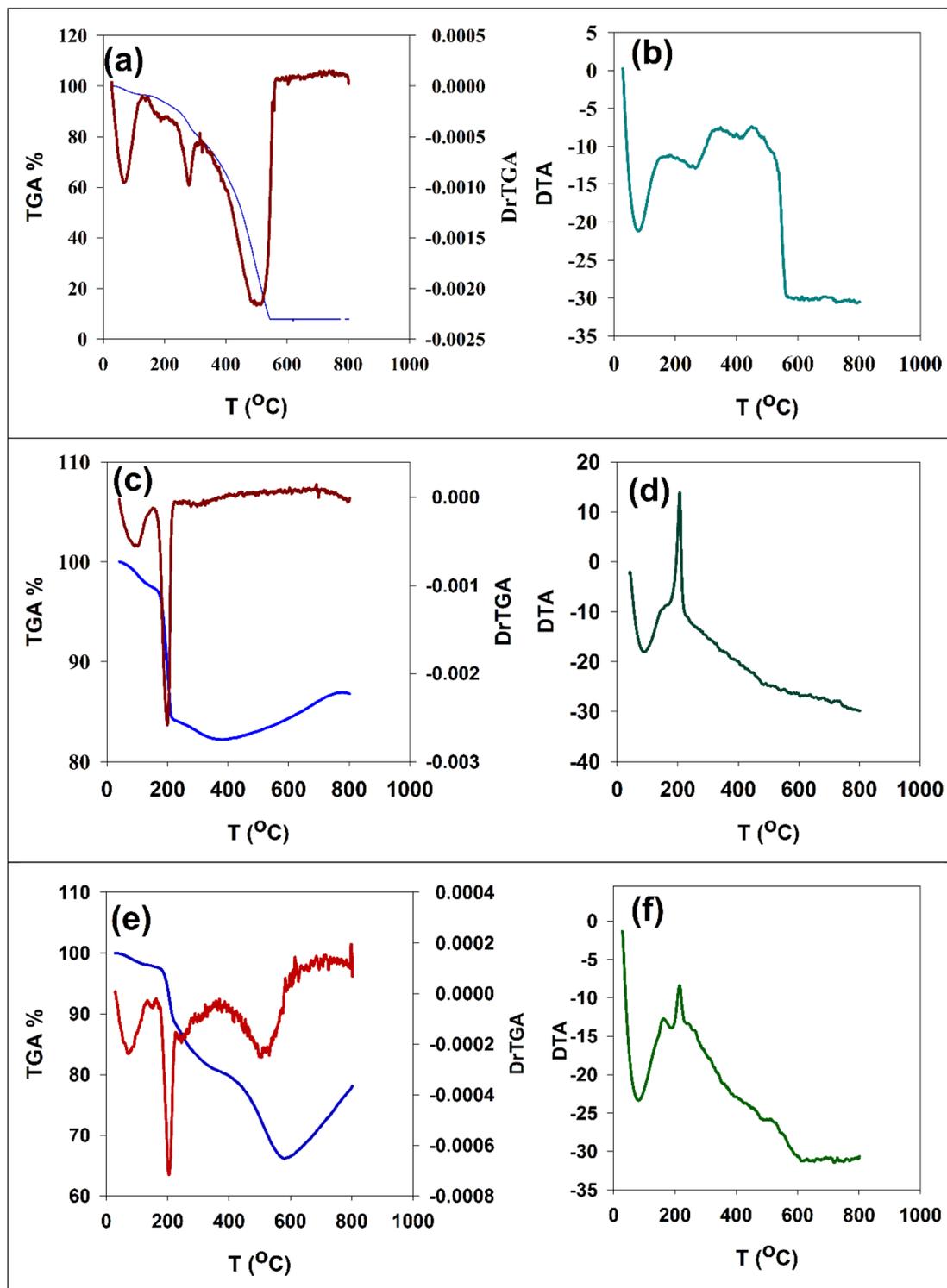

Fig. 4   (a and b) TGA & TDA curves of the poly aniline, (c and d) TGA & TDA curves of cobalt oxide, while (e and f) TGA & TDA curves of Pani & cobalt oxide.

sample. Downward peaks indicate endothermic processes, which are heat-absorbing, while upward peaks indicate exothermic processes, which are heat-releasing, possibly due to crystallization, oxidation, or decomposition reactions. Overall, the TGA curve reveals the thermal stability of polyaniline, with major decomposition occurring in the 200–600 °C range. The DrTGA curve helps identify the specific temperatures at which decomposition processes are most rapid. Fig. 4c and d present cobalt oxide's TGA/DrTGA and DTA curves. The TGA shows a relatively stable weight up to around 200 °C, indicating thermal stability. A significant weight loss occurs between 200–300 °C, suggesting a possible phase change or oxygen release. A subsequent gradual weight increase above 300 °C is unusual, potentially indicating oxidation or a reaction with the atmosphere. The DrTGA highlights the rate of these changes. Meanwhile, in DTA, an endothermic peak around 100 °C suggests a heat-absorbing process (*e.g.*, water loss). An exothermic peak around 250 °C aligns with the weight loss in TGA, indicating a heat-releasing reaction. A broad exothermic feature above 300 °C correlates with the weight increase in TGA. In summary, these curves show cobalt oxide's thermal behavior, including potential phase changes, oxygen release, and an unusual weight gain at higher temperatures. Further analysis is needed to determine the exact nature of these changes. Fig. 4e and f show the TGA/DrTGA and DTA curves for a composite of polyaniline (Pani) and cobalt oxide. The TGA curve shows a multi-stage weight loss. An initial loss below 200 °C is likely due to moisture or solvent. A significant weight loss occurs between 200–600 °C, indicating the decomposition of polyaniline. The DrTGA highlights the rate of these weight losses, showing peaks corresponding to the most rapid decomposition. A slight weight gain above 600 °C could indicate oxidation or a reaction with the atmosphere. In DTA curve, an endothermic peak around 100 °C suggests a heat-absorbing process like moisture loss. A large exothermic peak around 250 °C indicates

a heat-releasing decomposition, likely of polyaniline. A broad exothermic feature above 300 °C correlates with the weight gain in TGA, suggesting an ongoing exothermic reaction or process. In summary, these curves indicate the thermal behavior of the Pani/cobalt oxide composite. The decomposition of polyaniline is evident, along with potential reactions of cobalt oxide at higher temperatures.[40,41]

Fig. 5a displays the FT-IR spectrum of polyaniline, showing the figure labels several peaks with their corresponding functional groups: N–H stretch (around 3300–3400 cm^{-1}): this peak indicates the presence of N–H bonds, characteristic of the amine groups in polyaniline. C–H stretch (aromatic ring, around 3000–3100 cm^{-1}): this peak is due to the stretching vibrations of C–H bonds in the aromatic rings of polyaniline. C=C stretch (benzenoid and quinoid rings, around 1500–1600 cm^{-1}): this peak indicates the presence of C=C double bonds in the benzenoid and quinoid rings of polyaniline, which are the characteristic structural features of the polymer. C–N stretch (around 1200–1300 cm^{-1}): this peak is due to the stretching vibrations of C–N bonds in the polymer backbone. C–H in-plane bending (around 1100–1200 cm^{-1}): this peak is due to the in-plane bending vibrations of C–H bonds in the aromatic rings. C–H out-of-plane bending (around 800–900 cm^{-1}): this peak is due to the out-of-plane bending vibrations of C–H bonds in the aromatic rings. The presence of the characteristic peaks (N–H, C–H aromatic, C=C, C–N) confirms the successful synthesis of polyaniline. Fig. 5b displays the FT-IR spectrum of cobalt oxide, The figure labels several peaks with their corresponding vibrational modes Co–O–H (around 900–1100 cm^{-1}): this peak indicates the presence of hydroxyl groups (O–H) bonded to cobalt atoms, which is often observed in metal oxides, especially those that may have surface hydration. Co–O–Co (around 500–600 cm^{-1}): this peak is due to the stretching vibrations of Co–O–Co bonds in the cobalt oxide lattice. Co–O (around 400–500 cm^{-1}): This peak indicates the presence of Co–
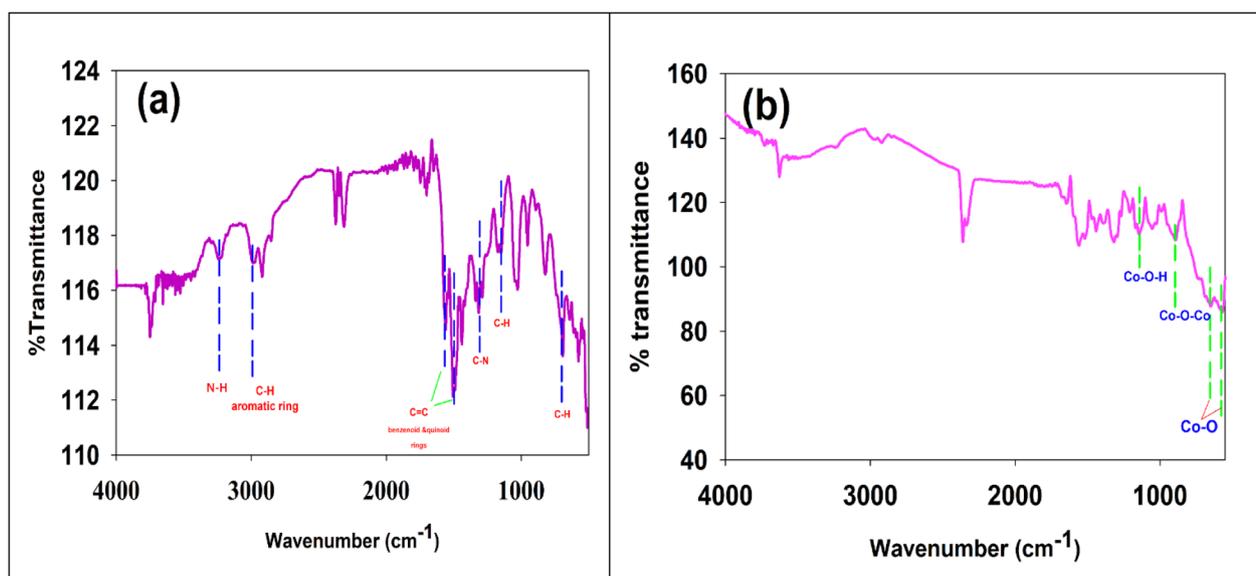

Fig. 5 (a) FT-IR of poly aniline (b) FT-IR of cobalt oxide.

O stretching vibrations, related to the fundamental metal–oxygen bonds in cobalt oxide. The presence of the characteristic peaks (Co–O–H, Co–O–Co, and Co–O) confirms the successful formation of cobalt oxide. The Co–O–H peak indicates the presence of surface hydroxyl groups, which are common in metal oxides and can affect their properties. The Co–O–Co and Co–O peaks provide evidence for the formation of the metal–oxygen bonds in the cobalt oxide lattice.[42]

By using a spectrophotometer, the UV-vis absorption spectra of polyaniline are captured at room temperature within the wavelength range of 200–1200 nm. Where, UV-visible spectroscopy is used to study the electronic transitions in a sample, providing information about its electronic structure and optical properties. Fig. 6a labels three distinct peaks at 314 nm, 609 nm, and 794 nm. 314 nm peak: this peak is typically associated with the π–π* transition in the benzenoid rings of polyaniline. It indicates the presence of conjugated double bonds in the polymer backbone. 609 nm peak: this peak is related to the polaron transition, characteristic of the doped or oxidized form of polyaniline. It indicates the presence of charge carriers (polarons) in the polymer. 794 nm peak: this peak is attributed to the bipolaron transition, which is also associated with the doped or oxidized form of polyaniline. It indicates the presence of higher energy charge carriers (bipolarons) in the polymer. The presence and relative intensities of the 609 nm and 794 nm peaks can provide information about the oxidation state of polyaniline. Higher intensities suggest a higher degree of doping or oxidation. The 314 nm peak provides information about the extent of conjugation in the polymer backbone. The UV spectrum of cobalt oxide nanoparticles exhibits two distinct absorption peaks at 307 nm and 498 nm, as shown in Fig. 6b. These peaks are indicative of electronic transitions within the material, specifically charge transfer and d–d transitions, respectively. Their positions and intensities provide insight into the electronic band gap, particle characteristics, and potential defects, all of which influence the optical properties of the cobalt oxide.[43]

3.2. Evaluation of the antimicrobial and antifungal effect: by well diffusion

The inhibitory zone diameter with standard deviations and means at cobalt oxide NPs along with polyaniline are shown in Table 1. The clear zone surrounding the wells indicated the antibacterial activity of cobalt oxide NPs. The best antibacterial activity with *Escherichia coli*, *Staphylococcus aureus*, and also *Bacillus subtilis* was demonstrated by the well diffusion method's zones of inhibition, which reached 22.0 ± 0.1 mm, 20.0 ± 0.1 mm, and 19.3 ± 0.6 mm, respectively. Also, the regions of inhibition in fungal activity reached to 20.3 ± 0.6 mm against *Candida albicans*. When a concentration of cobalt oxide NPs of 100 μg mL^{-1} was used. Whilst for 100 μg mL^{-1} of polyaniline the largest inhibitory zone against *Escherichia coli* was observed measuring 10.1 ± 0.1 mm in diameter. Whereas, there is no inhibition was seen with *Bacillus subtilis*, *Candida albicans*, or *Staphylococcus aureus*. Examples of inhibitory zones for various microorganisms are shown in Fig. 7. These findings concurred with those of Satpathy G., Manikandan E.,[36] and Moradpoor *et al.*,[44] who used the wells diffusion technique to reveal that cobalt oxide NPs and polyaniline exhibited antibacterial and antifungal action when exposed to harmful bacteria and fungi.

3.3. Electrochemical detection of nitrite upon Pani/Co$_2$O$_3$-NF

Using the cyclic voltammetry (CV) method, a powerful electrochemical technique used to study the redox behavior of electroactive species, we can detect the nitrite ions. In our study, it's being used to investigate the electrochemical oxidation of
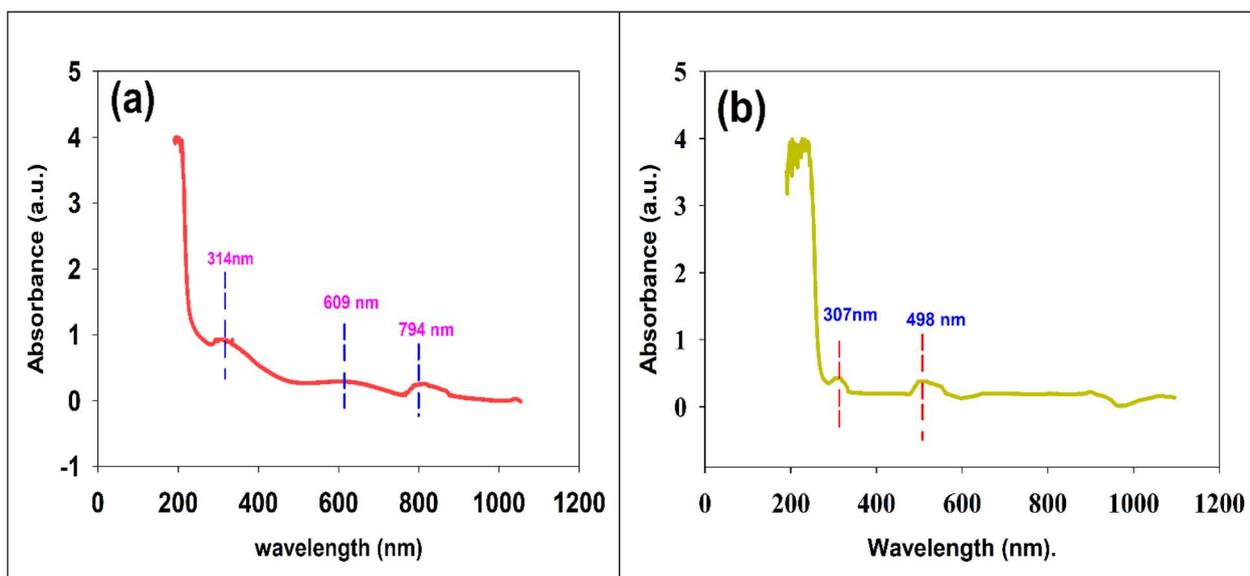

Fig. 6 (a) Illustrate UV-visible spectrum of poly aniline, (b) UV-visible spectrum of cobalt-oxide nanoparticles.

Table 1 Representation of polyaniline and cobalt oxide nanoparticles' antibacterial and antifungal properties utilizing the well diffusion technique

Sample microorganism	Polyaniline	Cobalt oxide NPs	Standard antibiotic
Gram negative bacteria			Gentamicin
Escherichia coli (ATCC:10536)	10.0 ± 1.0	22.0 ± 1.0	27.3 ± 0.6
Gram positive bacteria			Ampicilin
Staphylococcus aureus (ATCC:13565)	NA	20.0 ± 1.0	21.3 ± 0.6
Bacilus Subtits (DSM:1088)	NA	19.3 ± 0.6	22.0 ± 1.0
Fungi			Nystatin
Candida albicans (ATCC:10231)	NA	20.3 ± 0.6	21.3 ± 0.6

nitrite on different electrodes. Fig. 8 compares three different electrodes, GC (glassy carbon), the base electrode material, GC/Pani (glassy carbon/polyaniline): glassy carbon is modified with a layer of polyaniline, a conductive polymer, and GC/Pani/

Co_2O_3-NF: glassy carbon modified with a composite of polyaniline and cobalt oxide nanoparticles. The experiment is conducted in a 0.1 M phosphate buffer (PBS) at pH 7, containing 0.1 mM nitrite with a scan rate about (20 mV s^{-1}). This relatively
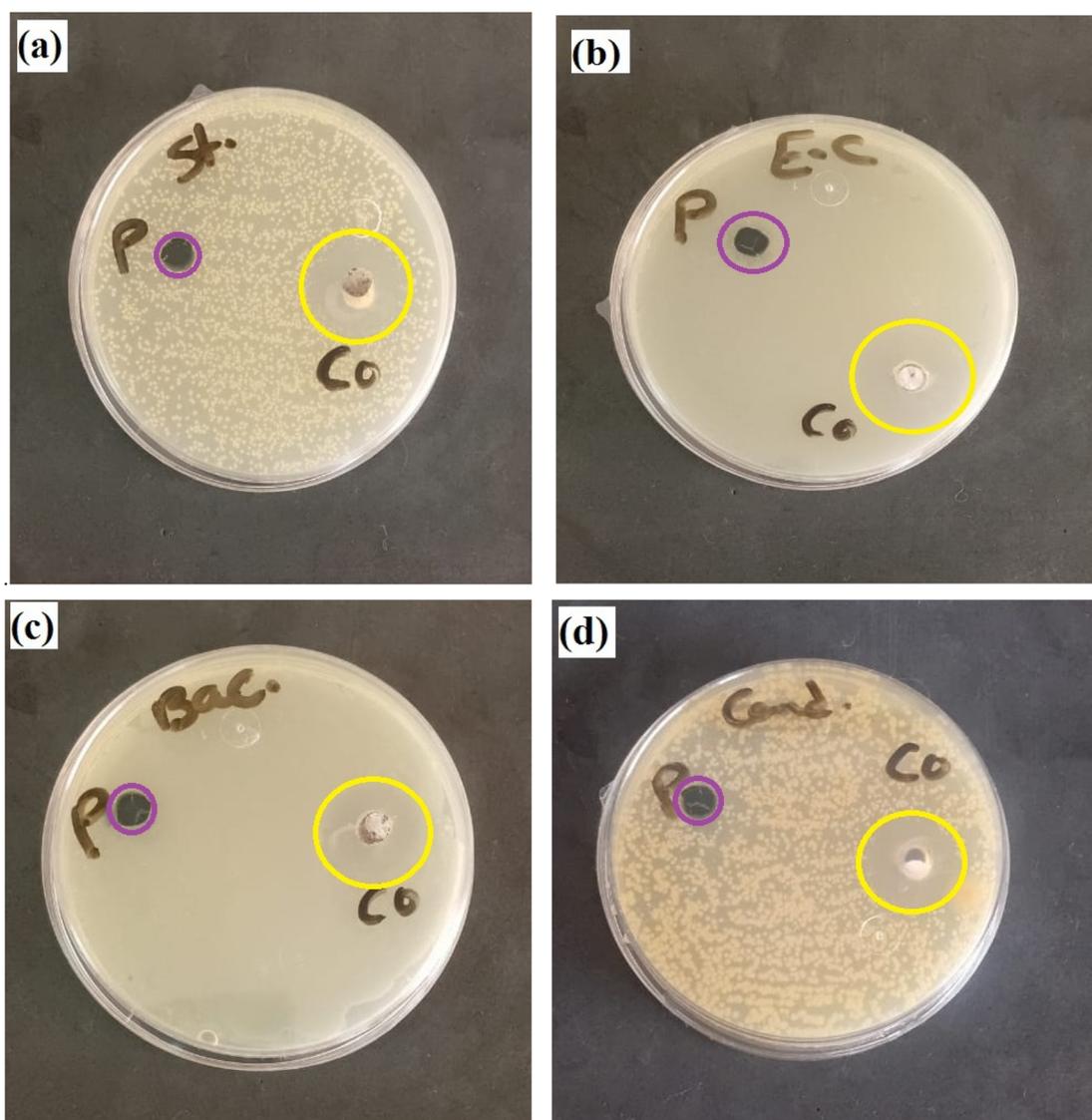
Fig. 7 Display bacterial inhibition zones. & additionally, isolates of fungus using 100 μg mL^{-1} of PANI and cobalt oxide NFs (a) *Staphylococcus aureus*, (b) *Escherichia coli*, (c) *Bacilus Subtits* and (d) *Candida albicans*.
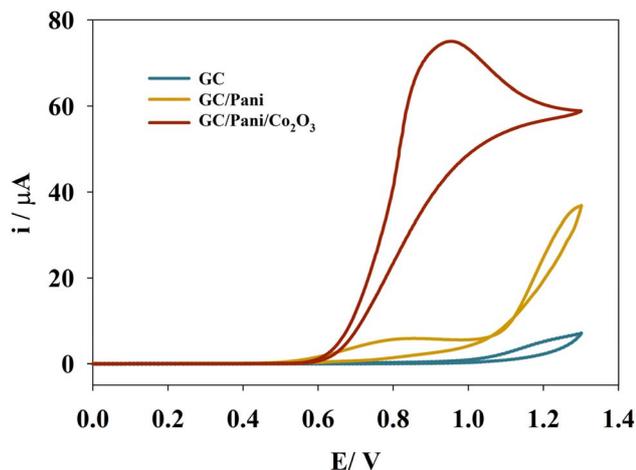
Fig. 8 The cyclic voltammetry of multiple electrodes (GC/Pani/Co$_2$O$_3$-NF, GC/Pani, and GC) in a solution of 0.1 M PBS (pH = 7) with 0.1 mM nitrite is shown at a scan rate of 20 mV s^{-1}.

conductivity of the electrode surface, facilitating electron transfer. Cobalt oxide is known to be an electrocatalyst for various redox reactions. It likely facilitates the electron transfer process involved in nitrite oxidation. The combination of polyaniline and cobalt oxide may lead to a synergistic effect, where the composite material exhibits enhanced properties compared to the individual components. Finally, GC/Pani/Co$_2$O$_3$-NF electrode exhibits the best electrocatalytic activity for nitrite oxidation among the tested electrodes. This suggests that this composite material is a promising candidate for developing electrochemical sensors for nitrite detection.[45] Interday stability of the GC/Pani/Co$_2$O$_3$-NF modified electrode was evaluated over 10 days. After this period, the electrode's activity decreased by 44%, and the significant drop in current indicates that the thin film gradually loses stability over time (see Fig. S1).

3.4. Effect of the number of cycles

To ascertain the ideal number of cycles for the altered electrode (GC/Pani/Co$_2$O$_3$-NF) for nitrite detection, the effect of number of cycles was studied. Fig. 9a displays the cyclic voltammograms of a modified electrode to adjust the electrochemical behavior of the electrode material over successive potential cycles. It is observed that the redox peaks increases with increase in cycle number. Initially, at 5 cycles, a relatively broad and less defined oxidation peak is seen around 1.0 V. As the number of cycles increases (10, 15, 20, and 25), the peak current gradually increases, suggesting an accumulation of electroactive species or changes in the electrode surface. The shape of the peak also appears to become sharper and more defined, indicating improved reversibility or faster electron transfer kinetics. The cathodic peak, though less pronounced, indicates a corresponding reduction process. The increase in peak current with cycling may be attributed to electrode activation, which increases the electroactive area, improves electron transfer, or to the formation/growth of an electroactive film on the electrode surface, enhancing the signal. Analyte accumulation on the

slow scan rate allows for the observation of diffusion-controlled processes. GC shows a low current response, indicating that nitrite oxidation is sluggish on bare glassy carbon. GC/Pani shows a slightly improved current response compared to GC, suggesting that polyaniline enhances nitrite oxidation. Otherwise, GC/Pani/Co$_2$O$_3$-NF exhibits a significantly larger current response, indicating a much more efficient nitrite oxidation process than the other electrodes. This suggests that cobalt oxide nanoparticles in the composite material greatly enhance electrocatalytic activity. So, the results demonstrate that modifying glassy carbon with polyaniline, especially with the polyaniline/cobalt oxide composite, significantly improves the electrochemical oxidation of nitrite. This is due to the enhanced surface area, where the composite material likely provides a larger surface area for the electrochemical reaction, leading to increased current. Polyaniline is a conductive polymer, and adding cobalt oxide nanoparticles may further enhance the
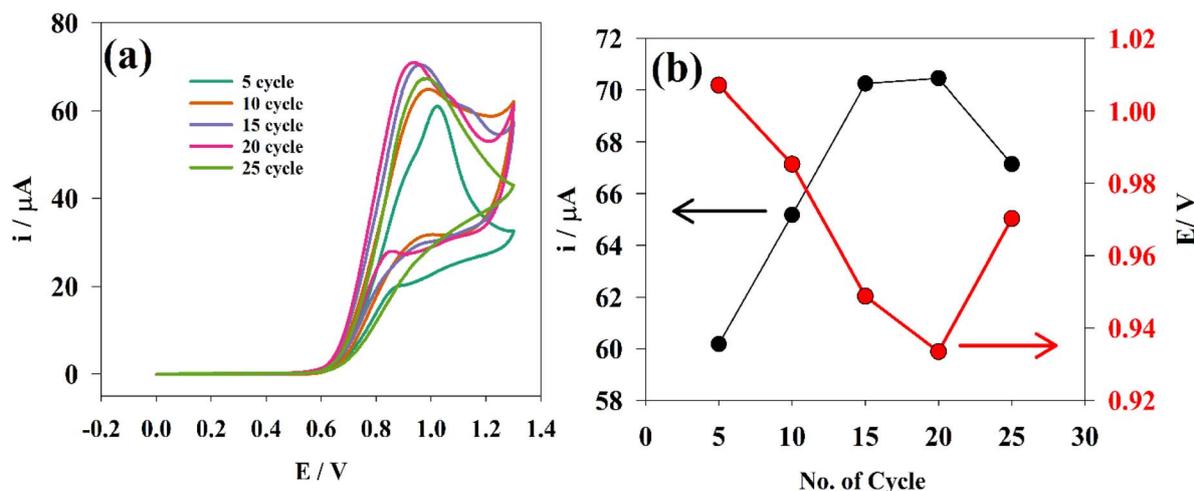

Fig. 9 (a) Represent the number of cycles by cyclic voltammetry of the modified electrode, (b) effect of cycles on oxidation current and potential.

electrode surface with each cycle, leads to a higher response. Fig. 9b presents the effect of the number of cycles on the peak current and the peak potential obtained from the cyclic voltammetry experiment. It was found that there is noticeable fluctuation in the current with increasing cycle numbers. Factors like surface changes, adsorption/desorption phenomena, or subtle changes in the electrode's environment might contribute to this behavior.

3.5. Effect of scan rate

The study evaluated the kinetic parameters of the nitrite oxidation process using a modified electrode. Fig. 10a represents the glassy carbon (GC) electrode modified with a composite of Polyaniline (Pani) and cobalt oxide (Co_2O_3) in an electrolytic solution of 0.05 M Phosphate Buffered Saline (PBS) and 0.1 mM nitrite (NO_2^-). The oxidation peak was observed at 0.6 V and increased as the potential was swept towards more positive values. The peak current increased with each successive scan. A reduction peak was observed on the reverse scan, indicating the reverse reaction of the oxidation reaction products. The increase in peak current with scan rate is a characteristic of a diffusion-controlled process, that indicates the reaction rate is governed by the mass-transfer of nitrite to the electrode surface. The shift in peak potential with scan rate provides information about the kinetics of the response, with a larger shift indicating a slower electron transfer rate. Fig. 10b examines the relationship between current and the square root of scan rate, revealing an upward trend as the square root of the scan rate increases. The relationship appears linear, especially in the higher scan rate region, with some curves having lower values. Randles–Sevcik describes this relationship:[14,46]

The Randles–Sevcik equation is:
$$i_p = (2.69 \times 10^5) \, n^{(3/2)} AD^{0.5} \, Cv^{0.5} \tag{3}$$

where: i_p is the peak current, n is the number of electrons transferred (here in this experiment $n = 1$), A is the electrode area, D is the diffusion coefficient, C is the concentration of the electroactive species, v is the scan rate.

This equation predicts a linear relationship between i_p and $v^{0.5}$, consistent with the observed trend equation, suggesting that the electrochemical reaction is primarily diffusion-controlled. The slight curvature in lower scan rate values could be due to other factors such as adsorption or kinetic limitations. The slope resulted from i_p–$v^{0.5}$ plot in this range can be used to calculate the diffusion coefficient (D), which indicates that the electrochemical reaction occurring at the electrode surface is primarily controlled by the diffusion process. Consiquently, the provided diffusion coefficient for modified electrode was $1.644 \times 10^{-4} \, cm^2 \, s^{-1}$. This information is crucial for understanding the mechanism and kinetics of the electrochemical reaction. Fig. 10b shows a linear relationship between the peak current and the square root of the scan rate, suggesting that the electrochemical reaction is diffusion-
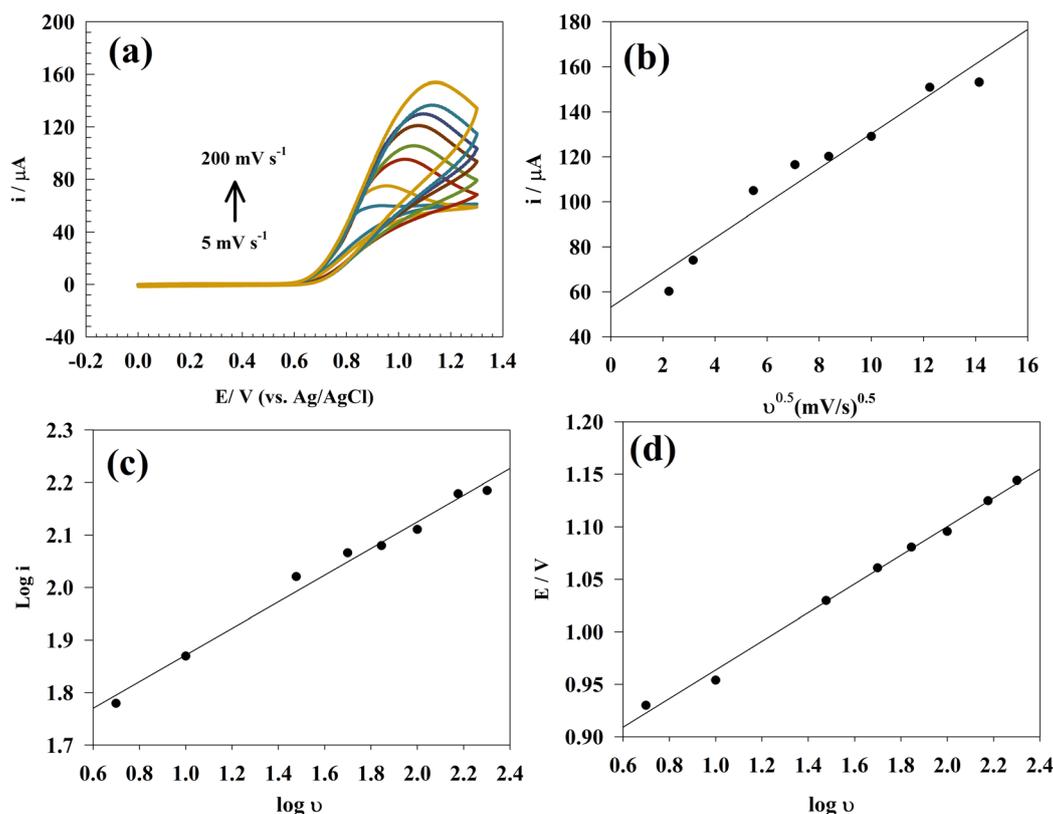

Fig. 10 (a) Represent the CVs of the GC/Pani/Co_2O_3-NF-modified electrode within 0.05 M PBS and 0.1 mM nitrite, (b) the relationship between current and the square root of scan rate, (c and d) the relationship between log scan rate with log current and the potential, respectively.

controlled. Fig. 10c illustrates the relationship between the logarithm of the scan rate ($\log \nu$) and the logarithm of the current ($\log i$) in an electrochemical experiment. The data points show a clear, linear, and upward trend. This positive correlation indicates that the increase in the scan rate increases the oxidation peak current. The linearity of this relationship is indicative of an adsorption-controlled process or a surface-confined electrochemical reaction. In such reactions, the current is not primarily limited by the diffusion of electroactive species from the bulk solution to the electrode surface, but rather by the electron transfer rate at the electrode surface where the electroactive species are adsorbed or confined. Fig. 10d illustrates the relationship between the logarithm of the scan rate ($\log \nu$) and the anodic peak potential (E). The graph shows that as the scan rate increases, the potential also tends to increase, but not perfectly linearly. This non-linear, upward trend suggests that the electrochemical reaction occurring at the electrode is not fully reversible. The potential would remain relatively constant regardless of the scan rate in an ideal reversible system. The observed change in potential with varying scan rates indicates that kinetic factors influence the reaction. Additionally, the potential gradually increases with increasing scan rate, suggesting that the reaction becomes more kinetically hindered. The non-linearity of the curve provides insights into the complexity of the electrochemical reaction.[47]

3.6. Effect changing of pH

Fig. 11a presents the cyclic voltammetry (CV) response of a GC/Pani/Co$_2$O$_3$-NF-modified electrode at various pH values, ranging from pH 2 to pH 10. It is crucial step in understanding the influence of pH on the electrochemical behavior of the modified electrode. The CV curves demonstrate a significant dependence of the electrochemical response on the pH of the solution. Both the anodic peak current and potential are affected by the change in pH. As the pH increases, there is a noticeable shift in the peak potential. This shift suggests that protons are involved in the electrochemical reaction. The relationship between peak potential and pH can provide insights into the proton-coupled electron

transfer (PCET) mechanism. The peak current also varies with pH, indicating that the electrode's reaction kinetics or surface activity is pH dependent. The peak current at pH 8 and 10 seems the highest, suggesting that the electrochemical reaction is most favorable in that pH range. Also, the variations in the CV curves at different pH values provide information about the stability and activity of the GC/Pani/Co$_2$O$_3$-NF modified electrode under various pH conditions. This is essential for practical applications where the electrode may be used in varying pH environments. The specific behavior observed is likely influenced by the properties of the GC/Pani/Co$_2$O$_3$-NF composite material. Polyaniline and cobalt oxide have pH-dependent electrochemical properties, contributing to the modified electrode's overall response. Fig. 11b illustrates the effect of pH on both the anodic peak current, and the potential. The data points reveal a complex relationship between pH and these electrochemical parameters, suggesting that the pH of the solution significantly influences the electrochemical process. The peak current at pH 8 shows that the reaction is most efficient at an alkaline pH. Meanwhile, the potential shows decreasing trend as the pH increases. This suggests that the electrochemical response is pH-dependent, and protons are likely involved. The decrease in potential with increasing pH indicates that the reaction becomes thermodynamically more favorable at higher pH values. This trend is an indication of a proton-coupled electron transfer reaction. So, it highlights the importance of controlling pH in electrochemical experiments, especially when studying proton transfer reactions. The results suggest that the electrode material or the electroactive species involved may change their properties as a function of pH.[48,49]

3.7. Electrochemical impedance spectroscopy

Electrochemical Impedance Spectroscopy (EIS) measurements, specifically focusing on the behavior of GC/Pani/Co$_2$O$_3$-NF modified electrode used for nitrite detection after different number of cycles is shown in Fig. 12. Each cycle (5, 10, 15, 20, and 25) corresponds to a different condition. Cycle 5 exhibits the highest charge transfer resistance value, indicating
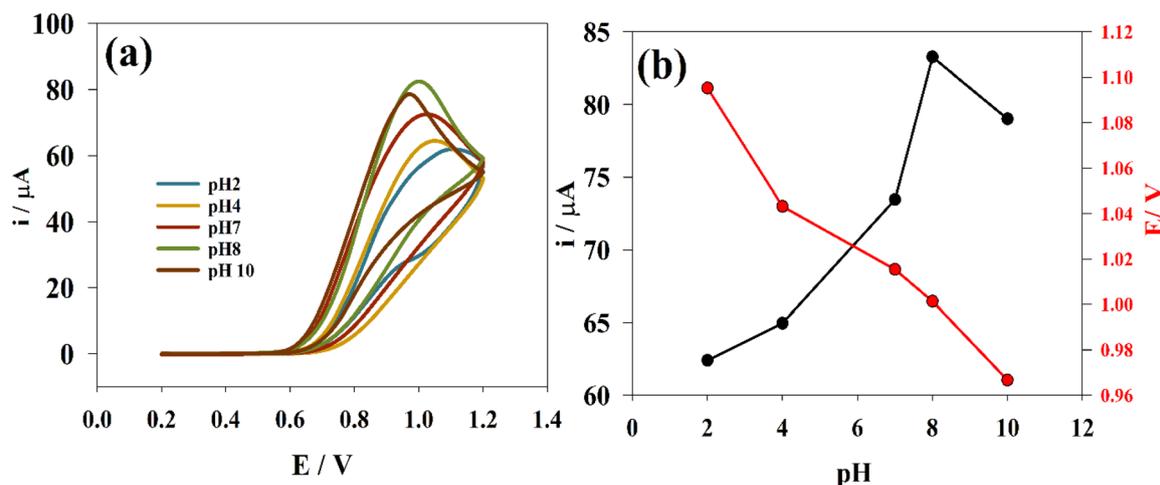

Fig. 11 (a) CVs of GC/Pani/Co$_2$O$_3$-NF at different pH, (b) effect of pH on anodic peak current and potential.

a significant resistance to charge transfer. The Nyquist plot shows a large semicircle, suggesting a high charge transfer resistance and considerable capacitance. From the electrochemical perspective, this indicates the worst efficiency for the electron transfer, and the electrode is at its lowest performance.

This is likely due to the initial interaction between the nitrite and the modified electrode, where the electrochemical system is unstable. However, cycle 15 exhibits the lowest charge transfer resistance values and the most minor semicircle diameter which indicates more electrochemical activity of the electrode. In summary, the graphs demonstrate a clear trend of decreasing impedance and improving electron transfer efficiency as the cycle number increases. This indicates that the electrochemical system becomes more optimized for nitrite detection with increasing cycles, with cycle 15 representing the optimal performance. The electrochemical fitting circuit is presented as an inset of Fig. 12. Table 2 represents fitting parameters for EIS data for different numbers of cobalt deposition cycles.
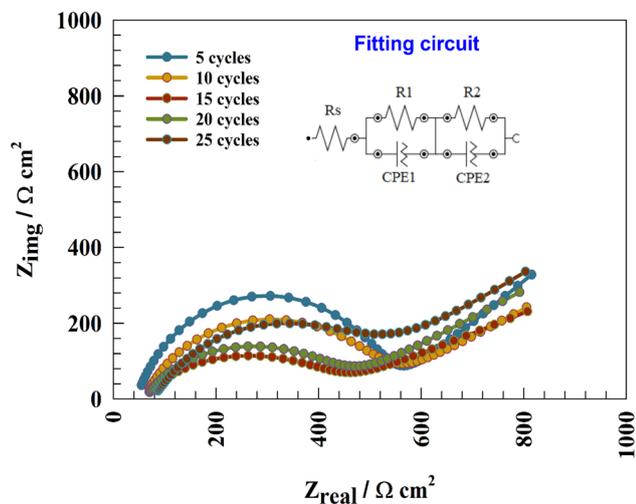
3.8. Impact of concentration of nitrite ions

The effect of nitrite concentration upon $GC/Pani/Co_2O_3$-NF was investigated to construct the calibration curve over a range of concentration (10 μM to 750 μM). Fig. 13a presents a comprehensive analysis of the modified electrode's ($GC/Pani/Co_2O_3$-NF) performance for sequential nitrite additions using chronoamperometry; the experiment was conducted in a PBS 0.1 M (pH 7) diluted solution at constant potential = 0.9 V (vs. Ag/AgCl). Fig. 13b presents the calibration curve, plotting the oxidation current against nitrite concentration. The electrode showed two linear ranges within low and high concentrations of nitrite. The first range of nitrite concentration was observed within (10 to 150) μM ($R^2 = 0.98$). The linear dynamic range was initially explored in the 0.1 mM to 0.5 mM range. The limit of detection (LOD) and limit of quantification (LOQ) can be calculated using the formulas $LOD = 3\ s\ m^{-1}$ and $LOQ = 10\ s\ m^{-1}$, where 's' and 'm' are the standard deviation and the calibration curve's slope, respectively. The LOD and LOQ were provided for low concentration of nitrite as (5.565 and 18.55) μM, respectively. On the other hand, the second linear concentration range was observed at higher nitrite concentration (200–750 μM) ($R^2 = 0.97$). The estimated LOD and LOQ

Fig. 12 Nyquist plots of $GC/Pani/Co_2O_3$-NF modified electrodes at various cycles (5, 10, 15, 20, and 25).

Table 2 EIS fitting parameters for different cycles of cobalt deposition

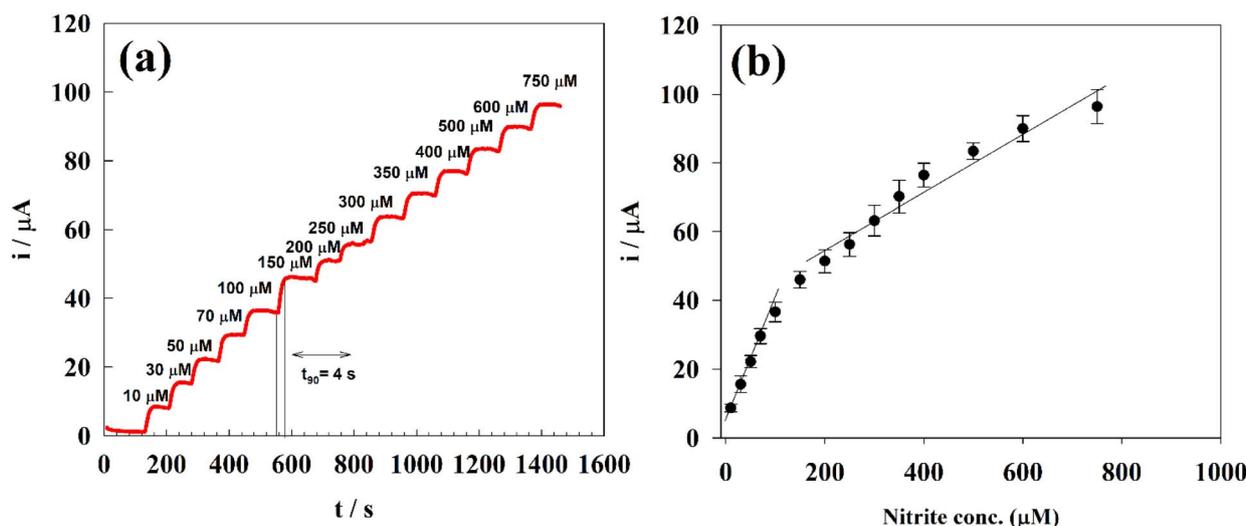| No. cycles	R_s ($\Omega\ cm^2$)	R_c ($\Omega\ cm^2$)	CPE Yo	CPE n	W ($\Omega\ s^{-1/2}$)
5	53	562	0.0000017	0.65	0.00000046
10	61	542	0.0000019	0.71	0.00000052
15	56	454	0.0000022	0.68	0.00000058
20	62	486	0.0000017	0.75	0.00000057
25	73	535	0.0000024	0.73	0.00000061

Fig. 13 (a) Chronoamperogram of response of the modified electrode for the gradual addition of nitrite ion, (b) the constructed calibration curve.

© 2025 The Author(s). Published by the Royal Society of Chemistry

were (44.98 and 149.9) μM, respectively. These parameters are crucial for assessing the suitability of the electrode for detecting nitrite in samples. Conclusion, Fig. 13a and b, along with the provided experimental details and calculations, provides a comprehensive evaluation of the GC/Pani/Co$_2$O$_3$-NF modified electrode for nitrite detection. The electrode exhibits a linear response within a specific concentration range and demonstrates good sensitivity, as evidenced by the calculated LOD and LOQ. This study highlights the potential of this electrode for practical applications in environmental monitoring.

3.9. Interference

Fig. 14 displays a chronoamperometric study to evaluate the anti-interference capabilities of a modified electrode (GC/Pani/Co$_2$O$_3$-NF) in the presence of various potentially interfering species. It was found to have an initial steady state at (0–200 s); the initial stable current indicates a baseline signal, likely representing the electrochemical detection of the target analyte or the establishment of a stable electrochemical process at the electrode surface. It was followed by interference at approximately 200 seconds, and a significant increase in current was observed. Group A introduces a mixture of amino acids (L-aspartic acid, L-methionine, L-asparagine, L-glutamic acid, and L-lysine), each at a concentration of 50 mM. After that, there is a constant current after interference, where the current, while

Fig. 14 Display of the modified electrode's anti-interference capabilities in various matrix types.

experiencing an initial jump, quickly stabilizes and remains relatively constant after adding the amino acids. This indicates that despite showing sensitivity to introducing these compounds, the electrode can maintain a stable signal, suggesting a degree of selectivity towards the target analyte. Further interference was added, such as salts (KCl and NaCl at 100 mM) and vitamin C (Group B). The resultant current also stayed constant, suggesting that the electrode also demonstrated good anti-interference capabilities in the presence of these species. The modified electrode exhibits sensitivity to amino acids, where the initial current jump demonstrates that the electrode is sensitive to the presence of amino acids. However, the stabilization of the signal indicates that the electrode's response is not permanently altered by their presence. The electrode's stability in the presence of salts and vitamin C suggests good anti-interference capabilities, which is crucial for accurate detection in complex biological or environmental samples. The electrode's ability to maintain a stable signal in the presence of interferents suggests that the modification layer or electrochemical process might involve a selective interaction with the target analyte, minimizing interference from other species. This suggests that the modification layer or electrochemical process might involve a selective interaction with the target analyte, minimizing interference from other species. Overall, the modified electrode's anti-interference capabilities demonstrate its potential for accurate detection in complex samples.
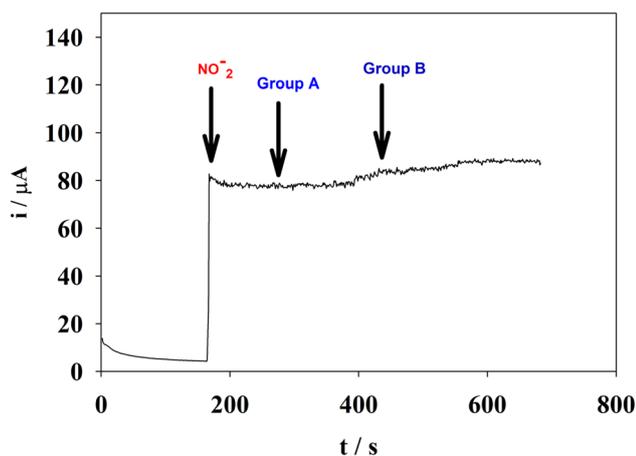
3.10. Analyses of real samples

The viability of GC/Pani/Co$_2$O$_3$-NF was assessed by identifying nitrite within apple juice and sausages through both an electrochemical analysis and High-Performance Liquid Chromatography (HPLC). Where two known amounts of nitrite were constantly added to the samples, and the findings were compared to the predicted values. To confirm the repeatability of the modified electrode (GC/Pani/Co$_2$O$_3$-NF), each experiment is conducted three times. According to Table 3, the initial concentration in both the electrochemical and HPLC methods detected the presence of nitrite in the sausage sample and apple juice. HPLC reported a slightly higher initial concentration of nitrite, about 1.69 mM and 0.11 mM, compared to the GC/Pani/Co$_2$O$_3$-NF electrode (1.41 mM) and (0.08 mM) for sausage and apple juice, respectively. By adding 2 mM nitrite, the nitrite

Table 3 Representing the recovery in sausage and apple juice sample for electrochemical and HPLC samples

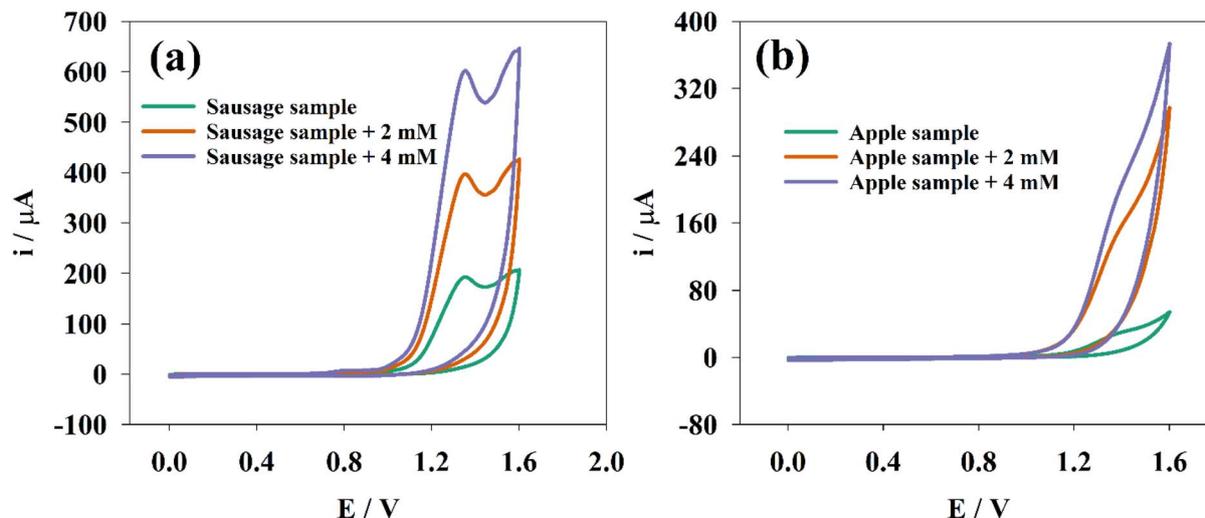| Sample	Electrochemical			HPLC		
	Conc. added	Concentration found (mM)	Recovery %	Conc. added	Concentration found (mM)	Recovery %
Sausage	—	1.41	—	—	1.69	—
	2 mM	3.36	98.5	2 mM	3.74	101.4
	2 mM	5.29	97.8	2 mM	5.81	102.1
Apple juice	—	0.08	—	—	0.11	—
	2 mM	2.05	98.6	2 mM	2.04	96.8
	2 mM	3.97	97.3	2 mM	4.1	99.7

Fig. 15 Representing of cyclic voltammetry for nitrite detection by using the (GC/Pani/Co$_2$O$_3$-NF) electrode, (a) in sausage samples, and (b) for apple juice samples.

Table 4 Representing comparison between some of different electrodes

Sensors	Sample	Linear range	Sensitivity	LOD	Ref.
PA-TaCoPC@ZnO	—	0.2–2 μM	6.3575 μA μM^{-1} cm^{-2}	21 nm	50
NMO/GF	Milk	100–5000 μM	0.146 μA μM^{-1}	1.36 μM	51
GCE/MWCNTs/AuNPs/PM	Milk, hawthorn juice	0.4–1475 μM	—	0.041 μM	52
GC/OD/FMWCNTs/p-ATT	Milk	10–1000 nM	—	0.2 nM	53
rGO-PE/pNR	Meat	0 : 14 000 μM	0.01511 μA μM^{-1}	17 nM	54
rGO/Pani/AsM	Water, cucumber, packaged drinks	25–7500 μM	0.803 μA μM^{-1} cm^{-2}	10.71 μM	55
AuNP/PCG/FTO	Grape, orange, apple juices	0–200 μM	0.63 μA μM^{-1} cm^{-2}	0.095 μM	56
NaCS-PDMDAAC-GCE	Ham sausage	0.04–150 μM	—	43 nM	57
Co$_3$O$_4$/Au/GCE	Commercial bottled water, beef	1–4000 μM	1.57 μA μM^{-1} cm^{-2}	0.11 μM	58
MoO$_3$–Co$_3$O$_4$-CC	Sausages, water	0.3125–11.5625 μM	1704.1 μA mM^{-1} cm^{-2}	0.075 μM	59
Co/PPy/GCE	Water and chinese cabbage pickled	2–3318 μM	2.60 μA μM^{-1} cm^{-2}	0.35 μM	60
GC/Pani/Co$_2$O$_3$-NF	Apple juice and sausage	(10–150) μM and (200–750) μM	0.0426 μA μM^{-1}	(18.55, and 149.9 μM)	This work

concentration was (3.36–2.05 mM) by the electrode (GC/Pani/Co$_2$O$_3$-NF), resulting in a recovery of 98.5–98.6% and (3.74–2.04 mM), by HPLC, resulting in a recovery of 101.4–96.8% for each of sausage and apple juice, respectively. Both methods show excellent recovery close to 100% at this spiking level. Then elevated the nitrite concentration by 2 mM again, (GC/Pani/Co$_2$O$_3$-NF) electrode measured (5.29–3.97 mM) from nitrite, resulting in a recovery of 97.8–97.3%. But by HPLC the concentration was (5.81–4.1 mM), resulting in a recovery of 102.1–99.7% for sausage and apple juice, respectively, as shown in Fig. 15, S2 and S3. Finally, these positive findings imply that in real-world applications, (GC/Pani/Co$_2$O$_3$-NF) modified electrode demonstrates outstanding nitrite detection efficiency and high reliability. Positive findings imply that GC/Pani/Co$_2$O$_3$-NF has outstanding nitrite detection capabilities and great

dependability in real-world applications. This study compared the results with the HPLC method using an HPLC chromatography YL-9100 system with C-18 (250 mm × 5 μm). The mobile phase used was methanol and deionized water in the ratio 50 : 50 at a 1 mL min^{-1} flow rate. The wavelength was fixed at 213 nm, and analyses were performed at the Microanalytical Center, Cairo University.

Furthermore, Table 4 included a comparison of our work with other papers that were included in the literature.

4. Conclusion

This study successfully developed and characterized a highly efficient electrochemical sensor for nitrite detection using a glassy carbon electrode modified with a polyaniline/cobalt

oxide nanocomposite (GC/Pani/Co$_2$O$_3$-NF). The antimicrobial and antifungal properties of both cobalt oxide and polyaniline were also evaluated, showing satisfactory activity and reinforcing their high sensitivity. Kinetic analyses indicated that nitrite oxidation is predominantly diffusion-controlled, with sensor performance strongly influenced by pH. The modified electrode further exhibited excellent anti-interference behavior against common interferents and demonstrated rapid, reliable performance in real food sample analysis. Overall, these results highlight the GC/Pani/Co$_2$O$_3$-NF electrode as a robust and efficient platform for nitrite detection, contributing significantly to food safety monitoring and environmental analysis. Future studies may focus on enhancing long-term stability, further optimizing performance, and expanding its applicability to more complex matrices.

Author contributions

Conceptualization: M. A. H., S. A. F., S. S. M.; methodology: N. I., M. A. H.; software: N. I., M. A. H.; formal analysis: N. I., M. A. H.; investigation: N. I., M. A. H., S. A. F., S. S. M.; resources: M. A. H., S. S. M.; writing – original draft: N. I.; writing – review & editing: N. I., M. A. H., S. S. M; visualization: N. I., M. A. H.; supervision: M. A. H., S. A. F., S. S. M.; project administration: M. A. H., S. A. F., S. S. M.; funding acquisition: M. A. H., S. S. M.

Conflicts of interest

The authors declare that they have no known competing financial interests or personal relationships that could have appeared to influence the work reported in this paper.

Data availability

The datasets utilized and analyzed during the current study can be obtained from the corresponding author upon request.

Supplementary information: the supplement file included HPLC curves for nitrite detection in real samples and interday stability for detection of nitrite using electrochemical method. See DOI: https://doi.org/10.1039/d5ra07841e.

References

1 K.-O. Honikel, The use and control of nitrate and nitrite for the processing of meat products, *Meat Sci.*, 2008, **78**, 68–76.

2 K. L. Jonvik, J. Nyakayiru, P. J. M. Pinckaers, J. M. G. Senden, L. J. C. van Loon and L. B. Verdijk, Nitrate-rich vegetables increase plasma nitrate and nitrite concentrations and lower blood pressure in healthy adults, *J. Nutr.*, 2016, **146**, 986–993.

3 L. Ma, L. Hu, X. Feng and S. Wang, Nitrate and nitrite in health and disease, *Aging Dis.*, 2018, **9**, 938.

4 M. Parvizishad, A. Dalvand, A. H. Mahvi and F. Goodarzi, A review of adverse effects and benefits of nitrate and nitrite in drinking water and food on human health, *Health Scope*, 2017, **6**, e14164.

5 J. Liu, Y. Chen, L. Wang, M. Na, H. Chen and X. Chen, Modification-free fabricating ratiometric nanoprobe based on dual-emissive carbon dots for nitrite determination in food samples, *J. Agric. Food Chem.*, 2019, **67**, 3826–3836.

6 M. Keerthi, S. Manavalan, S.-M. Chen and P.-W. Shen, A facile hydrothermal synthesis and electrochemical properties of manganese dioxide@graphitic carbon nitride nanocomposite toward highly sensitive detection of nitrite, *J. Electrochem. Soc.*, 2019, **166**, B1245.

7 W. J. R. Santos, P. R. Lima, A. A. Tanaka, S. M. C. N. Tanaka and L. T. Kubota, Determination of nitrite in food samples by anodic voltammetry using a modified electrode, *Food Chem.*, 2009, **113**, 1206–1211.

8 F. Gassara, A. P. Kouassi, S. K. Brar and K. Belkacemi, Green alternatives to nitrates and nitrites in meat-based products-a review, *Crit. Rev. Food Sci. Nutr.*, 2016, **56**, 2133–2148.

9 A. A. Avery, Infantile methemoglobinemia: reexamining the role of drinking water nitrates, *Environ. Health Perspect.*, 1999, **107**, 583–586.

10 M. R. Khan, S. M. Wabaidur, Z. A. Alothman, R. Busquets and M. Naushad, Method for the fast determination of bromate, nitrate and nitrite by ultra performance liquid chromatography-mass spectrometry and their monitoring in Saudi Arabian drinking water with chemometric data treatment, *Talanta*, 2016, **152**, 513–520.

11 A. Antczak-Chrobot, P. Bąk and M. Wojtczak, The use of ionic chromatography in determining the contamination of sugar by-products by nitrite and nitrate, *Food Chem.*, 2018, **240**, 648–654.

12 R. A. Soomro, S. Jawaid, P. Zhang, X. Han, K. R. Hallam, S. Karakuş, A. Kilislioğlu, B. Xu and M. Willander, NiWO$_4$-induced partial oxidation of MXene for photo-electrochemical detection of prostate-specific antigen, *Sens. Actuators, B*, 2021, **328**, 129074, DOI: 10.1016/j.snb.2020.129074.

13 N. S. Al-Kadhi, M. A. Hefnawy, S. S. Nafee, F. S. Alamro, R. A. Pashameah, H. A. Ahmed and S. S. Medany, Zinc Nanocomposite Supported Chitosan for Nitrite Sensing and Hydrogen Evolution Applications, *Polymers*, 2023, **15**(10), 2357, DOI: 10.3390/POLYM15102357.

14 S. S. Medany, M. A. Hefnawy, S. A. Fadlallah and R. M. El-Sherif, Zinc oxide–chitosan matrix for efficient electrochemical sensing of acetaminophen, *Chem. Pap.*, 2024, **78**, 3049–3061, DOI: 10.1007/s11696-023-03292-3.

15 N. Ezzat, M. A. Hefnawy, S. A. Fadlallah, R. M. El-Sherif and S. S. Medany, Synthesis of nickel-sphere coated Ni–Mn layer for efficient electrochemical detection of urea, *Sci. Rep.*, 2024, **14**, 14818, DOI: 10.1038/s41598-024-64707-z.

16 Z. H. Ibupoto, A. Nafady, R. A. Soomro, Sirajuddin, S. T. Hussain Sherazi, M. I. Abro and M. Willander, Glycine-assisted synthesis of NiO hollow cage-like nanostructures for sensitive non-enzymatic glucose sensing, *RSC Adv.*, 2015, **5**, 18773–18781, DOI: 10.1039/C4RA15858J.

17 M. A. Hefnawy, R. Abdel-Gaber, S. M. Gomha, M. E. A. Zaki and S. S. Medany, Green Synthesis of Cobalt Oxide Decorated Chitosan Substrates for Electrochemical

Detection of Nitrite and Hydrogen Evolution Reactions, *Electrocatalysis*, 2024, **15**, 496–506, DOI: 10.1007/s12678-024-00889-4.

18 N. Ibrahim, M. A. Hefnawy, S. A. Fadlallah and S. S. Medany, Recent advances in electrochemical approaches for detection of nitrite in food samples, *Food Chem.*, 2024, 140962.

19 N. S. Al-Kadhi, M. A. Hefnawy, F. S. Alamro, M. A. Ahmed, R. AL-Faze, A. M. Mostafa, H. A. Ahmed and S. S. Medany, Nickel–Manganese spinel oxide nanoparticles on graphite felt for ultrasensitive nitrite detection in milk samples, *Microchem. J.*, 2025, **213**, 113844, DOI: 10.1016/j.microc.2025.113844.

20 R. A. Soomro, J. Kumar, R. R. Neiber, Sirajuddin, A. M. Alotaibi, S. F. Shaikh, N. Ahmed and A. Nafady, Natural oxidation of $Ti_3C_2T_x$ to construct efficient TiO_2/$Ti_3C_2T_x$ photoactive heterojunctions for advanced photoelectrochemical biosensing of folate-expressing cancer cells, *Anal. Chim. Acta*, 2023, **1251**, 341016, DOI: 10.1016/j.aca.2023.341016.

21 M. H. Naveen, N. G. Gurudatt and Y.-B. Shim, Applications of conducting polymer composites to electrochemical sensors: a review, *Appl. Mater. Today*, 2017, **9**, 419–433.

22 M. H. Naveen, N. G. Gurudatt and Y.-B. Shim, Applications of conducting polymer composites to electrochemical sensors: a review, *Appl. Mater. Today*, 2017, **9**, 419–433.

23 J. Kim, R. Kumar, A. J. Bandodkar and J. Wang, Advanced materials for printed wearable electrochemical devices: a review, *Adv. Electron. Mater.*, 2017, **3**, 1600260.

24 N. S. Al-Kadhi, M. A. Hefnawy, F. S. Alamro, R. A. Pashameah, H. A. Ahmed and S. S. Medany, Polyaniline-supported nickel oxide flower for efficient nitrite electrochemical detection in water, *Polymers*, 2023, **15**, 1804.

25 X. Shi, W. Wei, Z. Fu, W. Gao, C. Zhang, Q. Zhao, F. Deng and X. Lu, Review on carbon dots in food safety applications, *Talanta*, 2019, **194**, 809–821.

26 K. Kawashima, R. A. Márquez, L. A. Smith, R. R. Vaidyula, O. A. Carrasco-Jaim, Z. Wang, Y. J. Son, C. L. Cao and C. B. Mullins, A review of transition metal boride, carbide, pnictide, and chalcogenide water oxidation electrocatalysts, *Chem. Rev.*, 2023, **123**, 12795–13208.

27 C. Das, N. Sinha and P. Roy, Transition metal non-oxides as electrocatalysts: advantages and challenges, *Small*, 2022, **18**, 2202033.

28 J. Zhang, B. Sun, X. Zhang, J. Gao, L. Zhang, C. Zhao and H. Suo, Simple and ultrasensitive self-supporting electrochemical sensor for nitrite based on cobalt oxide grafted carbon cloth, *Mater. Chem. Phys.*, 2023, **303**, 127763.

29 Y. Haldorai, J. Y. Kim, A. T. E. Vilian, N. S. Heo, Y. S. Huh and Y.-K. Han, An enzyme-free electrochemical sensor based on reduced graphene oxide/Co_3O_4 nanospindle composite for sensitive detection of nitrite, *Sens. Actuators, B*, 2016, **227**, 92–99.

30 J. Kumar, R. R. Neiber, A. Nafady, M. D. Albaqami, R. A. Soomro, M. Baraka, N. Ahmed and S. Karakuş, Robust Electrochemical Sensors for Detection of Isoprenaline Using Hexagonal Co_3O_4 Nanoplates Embedded in Few-Layer $Ti_3C_2T_x$ Nanosheets, *ACS Appl. Nano Mater.*, 2022, **5**, 11352–11360, DOI: 10.1021/acsanm.2c02445.

31 H. Liu, Q. Li, S. Zhang, R. Yin, X. Liu, Y. He, K. Dai, C. Shan, J. Guo and C. Liu, Electrically conductive polymer composites for smart flexible strain sensors: a critical review, *J. Mater. Chem. C*, 2018, **6**, 12121–12141.

32 F. Zhao, Y. Shi, L. Pan and G. Yu, Multifunctional nanostructured conductive polymer gels: synthesis, properties, and applications, *Acc. Chem. Res.*, 2017, **50**, 1734–1743.

33 N. F. Attia, K. A. Hady, S. E. A. Elashery, H. M. Hashem, H. Oh, A. M. Refaat and A. A. Hady, Greener synthesis route and characterization of smart hybrid graphene based thin films, *Surf. Interfaces*, 2020, **21**, 100681, DOI: 10.1016/j.surfin.2020.100681.

34 P. Kannusamy and T. Sivalingam, Chitosan–ZnO/polyaniline hybrid composites: polymerization of aniline with chitosan–ZnO for better thermal and electrical property, *Polym. Degrad. Stab.*, 2013, **98**, 988–996, DOI: 10.1016/j.polymdegradstab.2013.02.015.

35 V. Gupta, V. Kant, A. K. Sharma and M. Sharma, Comparative assessment of antibacterial efficacy for cobalt nanoparticles, bulk cobalt and standard antibiotics: a concentration dependant study, *Nanosyst.:Phys., Chem., Math.*, 2020, **11**, 78–85.

36 G. Satpathy and E. Manikandan, Cobalt nanoparticle as the antibacterial tool, *Int. J. Eng. Adv. Technol.*, 2019, **8**, 3684–3687.

37 B. A. Omran, H. N. Nassar, S. A. Younis, R. A. El-Salamony, N. A. Fatthallah, A. Hamdy, E. H. El-Shatoury and N. S. El-Gendy, Novel mycosynthesis of cobalt oxide nanoparticles using *Aspergillus brasiliensis* ATCC 16404—optimization, characterization and antimicrobial activity, *J. Appl. Microbiol.*, 2020, **128**, 438–457.

38 A. A. Abass, W. K. Alaarage, N. H. Abdulrudha and J. Haider, Evaluating the antibacterial effect of cobalt nanoparticles against multi-drug resistant pathogens, *J Med Life*, 2021, **14**, 823.

39 J. Iqbal, A. Numan, M. Omaish Ansari, R. Jafer, P. R. Jagadish, S. Bashir, P. M. Z. Hasan, A. L. Bilgrami, S. Mohamad and K. Ramesh, Cobalt oxide nanograins and silver nanoparticles decorated fibrous polyaniline nanocomposite as battery-type electrode for high performance supercapattery, *Polymers*, 2020, **12**, 2816.

40 Y. Teng, S. Yamamoto, Y. Kusano, M. Azuma and Y. Shimakawa, One-pot hydrothermal synthesis of uniformly cubic Co_3O_4 nanocrystals, *Mater. Lett.*, 2010, **64**, 239–242.

41 E. D. Lester, G. Aksomaityte, J. Li, S. Gomez, J. Gonzalez-Gonzalez and M. Poliakoff, Controlled continuous hydrothermal synthesis of cobalt oxide (Co_3O_4) nanoparticles, *Prog. Cryst. Growth Charact. Mater.*, 2012, **58**, 3–13.

42 M. Haridevi, S. Prabu, M. Lakshmi Devi, E. Bhakya Lakshmi, K. Mohanraj, A. Arun and M. Kayalvizhi, Synthesis and

characterization polyaniline/cobalt oxide nanocomposite by chemical oxidation method, *Nanoscale Rep.*, 2018, **1**, 9–20.

43 R. Bhargava, S. Khan, N. Ahmad and M. M. N. Ansari, Investigation of structural, optical and electrical properties of Co_3O_4 nanoparticles, in *AIP Conference Proceedings*, AIP Publishing, 2018.

44 H. Moradpoor, M. Safaei, F. Rezaei, A. Golshah, L. Jamshidy, R. Hatam and R. S. Abdullah, Optimisation of cobalt oxide nanoparticles synthesis as bactericidal agents, *Open Access Maced. J. Med. Sci.*, 2019, **7**, 2757.

45 M. Zhang, Y. Yang and W. Guo, Electrochemical sensor for sensitive nitrite and sulfite detection in milk based on acid-treated $Fe_3O_4@SiO_2$ nanoparticles, *Food Chem.*, 2024, **430**, 137004.

46 A. H. Bashal, M. A. Hefnawy, H. A. Ahmed, M. A. El-Atawy, R. A. Pashameah and S. S. Medany, Green synthesis of $NiFe_2O_4$ nano-spinel oxide-decorated carbon nanotubes for efficient capacitive performance—Effect of electrolyte concentration, *Nanomaterials*, 2023, **13**, 2643.

47 N. S. Al-Kadhi, M. A. Hefnawy, F. S. Alamro, R. A. Pashameah, H. A. Ahmed and S. S. Medany, Polyaniline-Supported Nickel Oxide Flower for Efficient Nitrite Electrochemical Detection in Water, *Polymers*, 2023, **15**, 1804, DOI: 10.3390/polym15071804.

48 Z. Akbari, M. Montazerozohori, G. Bruno, K. Moulaee and G. Neri, Development of a novel electrochemical nitrite sensor based on Zn-Schiff base complexes, *Appl. Organomet. Chem.*, 2022, e6610.

49 E. Saeb and K. Asadpour-Zeynali, A novel ZIF-8@ZIF-67/Au core–shell metal organic framework nanocomposite as a highly sensitive electrochemical sensor for nitrite determination, *Electrochim. Acta*, 2022, **417**, 140278, DOI: 10.1016/j.electacta.2022.140278.

50 S. M. Sudhakara, M. C. Devendrachari, F. Khan, S. Thippeshappa and H. M. N. Kotresh, Highly sensitive and selective detection of nitrite by polyaniline linked tetra amino cobalt(II) phthalocyanine surface functionalized ZnO hybrid electrocatalyst, *Surf. Interfaces*, 2023, **36**, 102565, DOI: 10.1016/j.surfin.2022.102565.

51 N. S. Al-Kadhi, M. A. Hefnawy, F. S. Alamro, M. A. Ahmed, R. AL-Faze, A. M. Mostafa, H. A. Ahmed and S. S. Medany, Nickel-Manganese spinel oxide nanoparticles on graphite felt for ultrasensitive nitrite detection in milk samples, *Microchem. J.*, 2025, **213**, 113844, DOI: 10.1016/j.microc.2025.113844.

52 E. Han, L. Li, T. Gao, Y. Pan and J. Cai, Nitrite determination in food using electrochemical sensor based on self-assembled MWCNTs/AuNPs/poly-melamine nanocomposite, *Food Chem.*, 2024, **437**, 137773.

53 K. Rajalakshmi and S. A. John, Highly sensitive determination of nitrite using FMWCNTs-conducting polymer composite modified electrode, *Sens. Actuators, B*, 2015, **215**, 119–124.

54 X. Guo and Y. Fan, Determination of nitrite in food specimens using electrochemical sensor based on polyneutral red modified reduced graphene oxide paste electrode, *Int. J. Electrochem. Sci.*, 2023, **18**, 100290.

55 B. P. Suma, P. S. Adarakatti, S. K. Kempahanumakkagari and P. Malingappa, A new polyoxometalate/rGO/Pani composite modified electrode for electrochemical sensing of nitrite and its application to food and environmental samples, *Mater. Chem. Phys.*, 2019, **229**, 269–278.

56 S. A. Ansari, N. S. Lopa, N. Parveen, A. A. Shaikh and M. M. Rahman, A highly sensitive poly (chrysoidine G)–gold nanoparticle composite based nitrite sensor for food safety applications, *Anal. Methods*, 2020, **12**, 5562–5571.

57 J. Ning, X. Luo, M. Wang, J. Li, D. Liu, H. Rong, D. Chen and J. Wang, Ultrasensitive electrochemical sensor based on polyelectrolyte composite film decorated glassy carbon electrode for detection of nitrite in curing food at sub-micromolar level, *Molecules*, 2018, **23**, 2580.

58 V. S. Manikandan, S. Durairaj, E. Boateng, B. Sidhureddy and A. Chen, Electrochemical detection of nitrite based on Co_3O_4–Au nanocomposites for food quality control, *J. Electrochem. Soc.*, 2021, **168**, 107505.

59 T. Zhe, M. Li, F. Li, R. Li, F. Bai, T. Bu, P. Jia and L. Wang, Integrating electrochemical sensor based on MoO_3/Co_3O_4 heterostructure for highly sensitive sensing of nitrite in sausages and water, *Food Chem.*, 2022, **367**, 130666.

60 H. Lü, H. Wang, L. Yang, Y. Zhou, L. Xu, N. Hui and D. Wang, A sensitive electrochemical sensor based on metal cobalt wrapped conducting polymer polypyrrole nanocone arrays for the assay of nitrite, *Microchim. Acta*, 2021, **189**, 26, DOI: 10.1007/s00604-021-05131-2.